

Architectures, electronic structures, and stabilities of Cu-doped Ge_n clusters: density functional modeling

Debashis Bandyopadhyay

Received: 28 June 2011 / Accepted: 2 February 2012 / Published online: 17 March 2012
© Springer-Verlag 2012

Abstract The present study reports the geometries, electronic structures, growth behavior, and stabilities of neutral and ionized copper-doped germanium clusters containing 1–20 Ge atoms within the framework of linear combination of atomic orbitals density functional theory (DFT) under the spin-polarized generalized gradient approximation. It was found that Cu-capped Ge_n (or Cu-substituted Ge_{n+1}) and Cu-encapsulated Ge_n clusters mostly occur in the ground state at a particular cluster size (n). In order to explain the relative stabilities of the ground-state clusters, parameters such as the average binding energy per atom (BE), the embedding energy (EE), and the fragmentation energy (FE) of the clusters were calculated, and the resulting values are discussed. To explain the chemical stabilities of the clusters, parameters such as the energy gap between the highest occupied and the lowest unoccupied molecular orbitals (the HOMO–LUMO gap), the ionization energy (IP), the electron affinity (EA), the chemical potential (μ), the chemical hardness (η), and the polarizability were calculated, and the resulting values are also discussed. Natural atomic orbital (NAO) and natural bond orbital (NBO) analyses were also used to determine the electron-counting rule that should be applied to the most stable Ge_{10}Cu cluster. Finally, the relevance of the calculated results to the design of Ge-based superatoms is discussed.

Keywords Clusters and nanoclusters · Binding energy · Density functional theory · Electron affinity · Embedding energy · Ionization potential

Introduction

Atomic clusters containing few to a few hundred atoms have attracted attention because of their importance in nanoscience and nanotechnology. These clusters are considered to be a new phase of matter with properties that are sensitive to the size and composition of the clusters. The novel physical and chemical properties of these nanoscale clusters could lead to many new and exciting applications. Many new fields of research have evolved that aim to probe and unravel the properties of the nanoclusters. Among these atomic clusters, pure and hybrid semiconductor nanoclusters have attracted a lot of theoretical and experimental attention due to their potential industrial applications [1–7]. However, pure semiconductor clusters are chemically reactive [8]. Hence, stabilizing these clusters is an important and major challenge before any application of them. The main cause of the instability or reactivity of semiconductor clusters is the presence of unsaturated dangling bonds in the cluster. Encapsulating one or more transition metal atoms inside the semiconductor cluster can saturate the dangling bonds and enhance the stability of the cluster [9, 10]. The exohedral addition of hydrogen atoms to pure or hybrid semiconductor clusters can also “tie up” the dangling bonds and improve the stability of these clusters [11]. It has been noted that the fullerene-like hydrogenated silicon cages of formula Si_nH_n with $n=20, 28, 30, 36, 50,$ and 60 are very stable with large HOMO–LUMO energy gaps, which makes them suitable for optoelectronic and other applications

D. Bandyopadhyay (✉)
Physics Department, Birla Institute of Technology and Science,
Pilani, Rajasthan 333031, India
e-mail: debashis.bandy@gmail.com

[8, 9, 12–16]. Important experimental contributions have been made by several research groups on the stability of transition metal doped semiconductor clusters. Using a laser vaporization supersonic expansion technique, Beck [17, 18] showed that the addition of transition metals such as Cr, Mo, and W to Si clusters enhanced the stability of the doped clusters compared to the pure Si clusters of the same size by subjecting them to photofragmentation. Hiura et al. [19] reported the formation of a series of stable transition metal doped Si cages. O'Hara et al. [20] studied the geometric and electronic structures of anionic Si_nTb clusters with photoelectron spectroscopy and a chemical probe method, and proved that the Tb atom always remains encapsulated inside Si_{10} clusters. Recently, Bandyopadhyay [21, 22] and Bandyopadhyay et al. [23–25] reported an extensive study of the electronic structures, growth behavior, and different physical and chemical properties of pure and transition metal doped Si and Ge clusters ($\text{TM}@M_n$ where $M = \text{Si}$ or Ge ; $\text{TM} = \text{Ti, Zr, Hf, V, Sc}$; $n = 1–20$). They found that metal-doped fullerenes such as $M_{16}\text{TM}$ (Si or Ge ; $\text{TM} = \text{Ti, Zr, Hf}$), Ge_{15}V , and Ge_{17}Sc clusters are the most stable chemically species among all of the clusters they studied. Recently, a detailed theoretical study of pure and hybrid Ge nanoclusters in neutral and cationic states was reported by Bandyopadhyay and Sen [26]. They found that the growth behavior of these clusters (Ge_n and Ge_nNi , $n = 1–20$) presents two different trends in two different size ranges. In the smaller size range ($n < 9$), the binding energy increases rapidly with cluster size and then tends to saturate in the larger size range ($n > 12$). Across the whole size range, Ge_{10}Ni , which is a 20-electron cluster, is the most stable species. Many experimental results on pure Ge clusters have been reported by several groups [27–31]. Some of recent investigations of pure and halogen-doped Ge clusters have mainly focused on optimized geometries, binding energies, ionization potentials, electron affinities, and so on [30, 31]. Other theoretical and experimental contributions from different groups have examined the endohedral doping of transition metal doped, hydrogenated, cage-like Ge clusters [32–35].

Although many extensive experimental and theoretical studies have been performed so far, one question has still not been adequately addressed: the science behind the stability of these nanoclusters. Depending upon their compositions, different neutral and charged clusters are stable at different sizes. An “electron-counting rule” is sometimes used to explain the stability of such clusters. In transition metal doped Si and Ge clusters, the stabilities of the clusters are often found to obey an 18-electron counting rule (also known as the “octet rule”) and sometimes a 20-electron counting rule [24–26, 36]. It is well known that cluster stability depends upon the nature of the transition metal used to dope the host semiconductor cluster. As example, according to the 18-electron rule, Si_{12}Cr and Si_{12}W should be the most stable clusters in the 3*d* and 5*d* transition metal doped Si_n series, respectively [10], whereas,

according to the 20-electron rule, $\text{TM}@M_{16}$ among the clusters $\text{TM}@M_n$ ($\text{TM} = \text{Ti, Zr, Hf}$; $M = \text{Si}$ or Ge) [21–24], Ge_{15}V , Ge_{17}Sc , and Ge_{10}Ni [25, 26] are the most stable structures across the whole size range ($n = 1–20$). Recent investigations have shown that an electron-counting rule cannot always explain the stabilities of some clusters [37, 38]. In addition to an electron-counting rule, it is sometimes necessary to apply the free-electron gas theory with the Wigner–Witmer (WW) spin conservation rule [39] to calculate the embedding energy (EE), which is one of the most important parameters for explaining the thermodynamic stabilities of clusters. Again, the free-electron gas picture is not valid in every case; for instance, the anionic clusters $\text{Mn}@Si_{12}$ and $\text{Co}@Si_{12}$ have the highest embedding energies even though they are 20- and 22-electron clusters, respectively [40]. On the other hand, Koyasu et al. [41] experimentally verified the validity of electron-counting rules by studying the electronic and geometric structures of Si_{16}Ti clusters using different spectroscopic techniques and demonstrating that neutral Si_{16}Ti (a 20-electron cluster) has a closed-shell electronic configuration with a large HOMO–LUMO gap. A large HOMO–LUMO gap always helps to increase cluster stability, as it reduces cluster reactivity. Recently, Bandyopadhyay and others [24–26] used DFT studies to show that $\text{TM}@M_n$ ($M = \text{Si}$ or Ge ; $\text{TM} = \text{Ti, Zr, Hf, Sc, V, Ni}$; $n = 1–20$) systems show the same behavior.

Following from the research described above on pure and transition metal doped Si and Ge clusters, the work described in the present paper was performed in an attempt to explain the enhanced stability of the Ge_{10}Cu cluster among the Ge_nCu ($n = 1–20$) series of clusters by studying the physical and chemical properties of all of the ground-state clusters in this series using density functional theory (DFT). Although such Ge_nCu ($n = 1–13$) clusters have already been studied theoretically [41], the clusters examined previously were much smaller than the size of a nano quantum dot. Therefore, the larger clusters studied in the present work have more practical relevance, and the results obtained here can be compared with the corresponding data obtained experimentally in the future. The main focus of the present study was to explain the thermodynamic stability of these clusters in their neutral and charged states along with their chemical properties in detail.

Computational

In the present work, all of the theoretical calculations were performed within the framework of linear combination of atomic orbitals density functional theory. The exchange-correlation potential contributions were incorporated into the calculation using the spin-polarized generalized gradient approximation (GGA) proposed by Perdew and Wang (B3PW91)

[42–45]. The standard Gaussian basis (LanL2DZ) was used to express the molecular orbitals (MOs) of all atoms as linear combinations of atom-centered basis functions. LanL2DZ is a double- ζ , 18-valence electron basis set with a LANL effective core potential (ECP) [46]. This basis set can reduce the difficulties associated with the two-electron integrals caused by the transition metal atoms [47–50]. All geometry optimizations were performed with no symmetry constraints. During optimization, it is always possible that a cluster with a particular guessed geometry can get trapped at a local minimum on the potential energy surface. To avoid this during the optimization of clusters of a particular size, several initial guessed geometries with different spin states (doublet to sextet) were used to search for the ground-state (GS) isomer. In order to check the validity of the applied methodology, a trial calculation was carried out on the Ge–Ge dimer. The calculated Ge–Ge bond length was 2.54 Å (with a frequency of 250.66 cm^{-1}), which is within the range of the values obtained theoretically as well as experimentally by Nagendran et al. [51]. The bond length of the Cu–Cu dimer obtained using the present method was 2.25 Å, and the corresponding frequency was 259.75 cm^{-1} . These are in good agreement with the experimental value for the bond length (2.22 Å) and the experimental frequency (266 cm^{-1}), respectively [52, 53]. Same calculations were also performed at the B3LYP/lanL2DZ and B3LYP/SDD (SDD is a triple- ζ , 18-valence electron basis set with the Stuttgart/Dresden effective core potential) levels. Comparing these results with those obtained at the B3PW91/LanL2DZ level of calculation, it was found that the values for the optimized bond lengths of the dimers obtained by the latter method were in better agreement with the experimental data. Therefore, in the present study, the B3PW91/LanL2DZ level of calculation was used. In a recent report, Wang and Chao [54] discussed the compatibilities of different methods that are used for Si and Ge clusters. In the present calculation, bearing in mind their calculation method, all of the ground-state geometries of the clusters with $n=1$ –20 obtained using B3PW91/LanL2DZ were checked at the B3LYP/LanL2DZ and B3LYP/SDD levels of calculation. The physical and chemical parameters of the clusters were found to behave in same manner at both levels of calculation. The optimized electronic structure was obtained by solving the Kohn–Sham equations self-consistently [55] using the default optimization criteria of the Gaussian 03 program [54]. The initial guessed geometries of the clusters were constructed on the basis of reported optimized geometries [26, 41] as well as intuition founded on the growth behavior of the clusters. To check the reliability of the optimized geometries, a frequency check calculation of the harmonic vibrations of the clusters was done. If an imaginary frequency was found in a particular vibrational mode, relaxation was performed along that mode until the true local minimum was obtained. Geometry optimizations were carried out to a convergence limit of 10^{-7} Ha in the total optimized energy. The optimized

geometries as well as the electronic properties of the clusters of each size were obtained from the calculated program output. All theoretical calculations were performed with the Gaussian 03 software package [56].

Results and discussion

In a previous report, a detailed discussion of the growth behavior of Ge_n clusters was presented [26]. In the present section, the growth behavior of Ge_nCu clusters will be discussed within the size range of $n=1$ –20 based on the calculated values of various parameters of the different optimized ground-state isomers at each size.

The first member of this series is the Ge–Cu dimer. The optimized structure has a doublet spin state with $C_{\infty v}$ point group symmetry. The bond length of the dipole is 2.36 Å and its frequency is 238.28 cm^{-1} . Adding a Ge atom to the optimized Ge–Cu dimer with no symmetry constraints leads to four possible geometries. The isomer with triangular geometry (2A), a doublet spin state, and C_{2v} point group symmetry (see Fig. 1a) is the ground state. The same structure also can be optimized by capping the Ge_2 dimer with a Cu atom or by replacing a Ge atom in Ge_3 that is in a triangular geometry with a Cu atom. Among the three remaining geometries, Ge–Cu–Ge is a bent structure (2B), while the other two are linear chain isomers (2C and 2D) with the Cu atom at different positions in the chain, as shown in Fig. 1a.

Three different geometries were optimized for the next cluster size, $n=3$. Two of them are arranged in a rhombus, while the third has a pyramid-like structure with a triangular Ge_3 base. This structure can be obtained by replacing a Ge atom in a planar Ge_4 rhombus structure with a Cu. Depending upon the position of the Cu atom, two different rhombi can be obtained. The first isomer (3A) shown in Fig. 1a is a bent rhombus with C_{2v} symmetry in a doublet spin state, and this isomer is higher in energy than the other planar rhombus geometry (3C). The latter rhombus structure can be obtained after optimizing a Cu-capped triangular Ge_3 structure in the same plane. In the 3A and 3C structures, the Ge–Ge–Ge angles are 129.77° and 65.72°, respectively, whereas the Ge–Cu–Ge angles are 114.18° and 67.86°.

Five stable structures were optimized for Ge_4Cu . The ground-state isomer (4A) shown in Fig. 1a is obtained by replacing the apical Ge atom in the Ge_5 pyramidal structure with C_{2v} symmetry while retaining its bent Ge_4 rhombus base, or by capping the planar Ge_4 rhombus with a Cu atom (in the optimized structure, the planar rhombus is transformed into a bent rhombus structure). The next isomer (4B), which as C_s symmetry, is a pentagon; see Fig. 1a. This structure can be obtained by capping the planar rhombus 3A in the same plane with a Ge atom on a Ge–Cu arm. The remaining three structures are of the same type (4C, 4D, and 4E). These structures

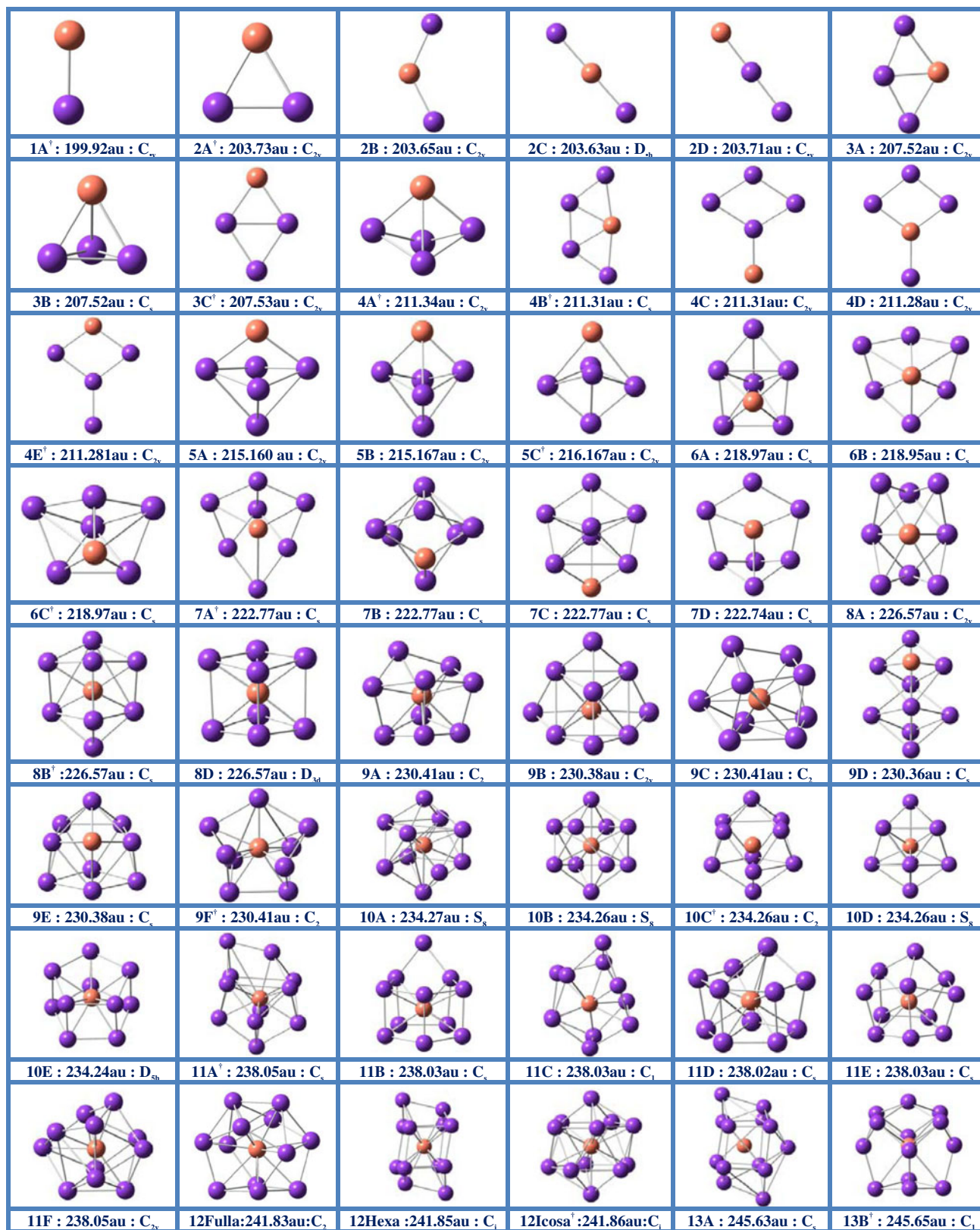
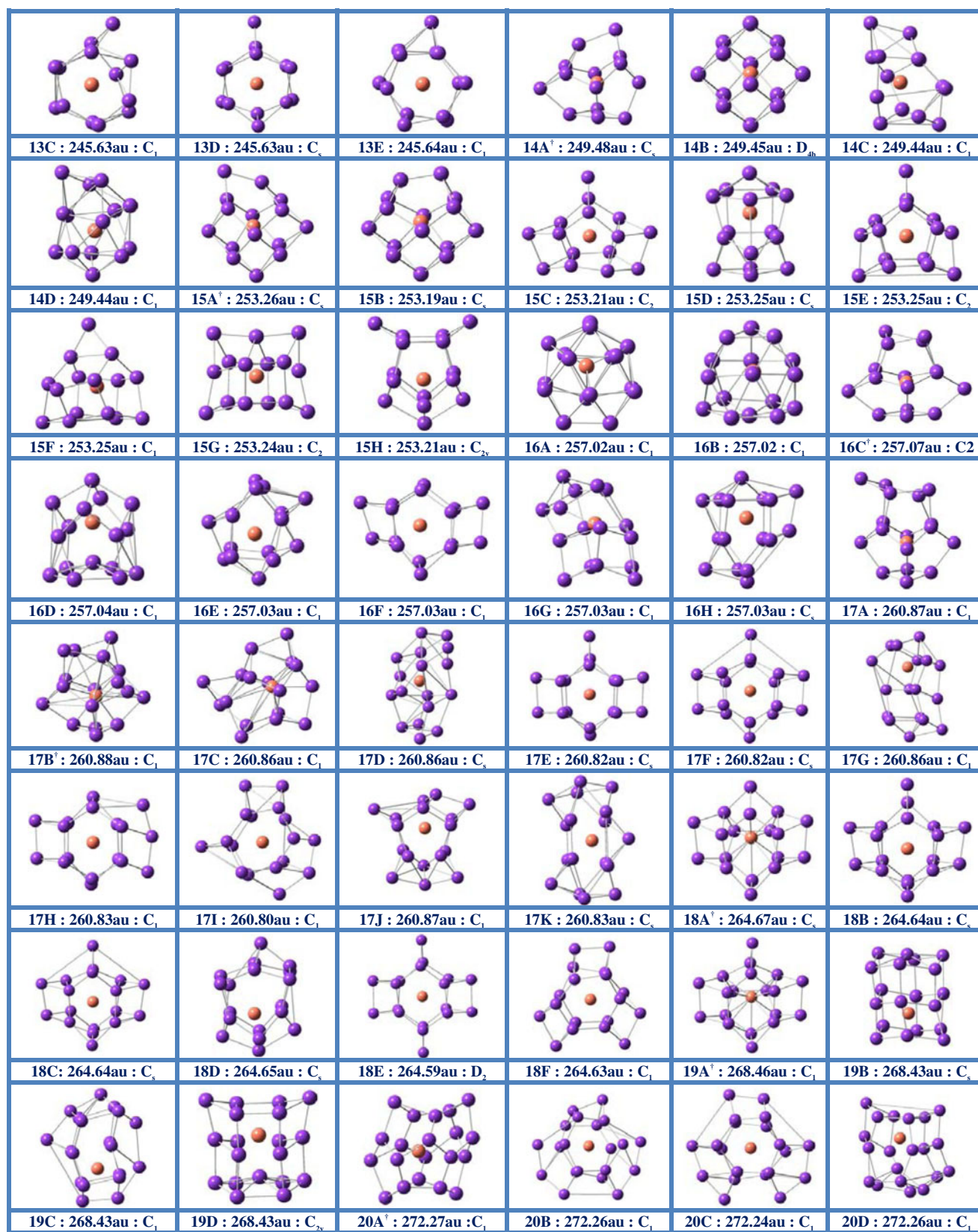
a

Fig. 1 a Optimized structures of neutral Ge_nCu ($n=1-20$) clusters, including their optimized energies and point group symmetries. **b** Contributions of the different valance orbitals of Ge and Cu atom(s)

to the HOMO of the Ge₁₀Cu icosahedral ground-state cluster, as obtained from NBO analysis. The *numbers below the clusters* represent the occupancies of the valance orbitals



*1 atomic unit (au)=27.212 eV; †ground state; optimized energies presented are rounded to two decimal places

Fig. 1 (continued)

b

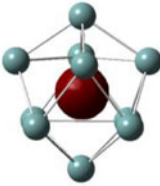
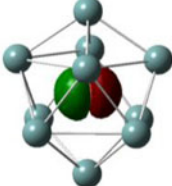
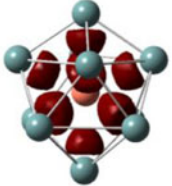
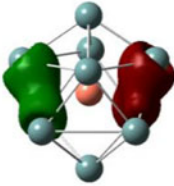
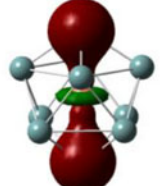
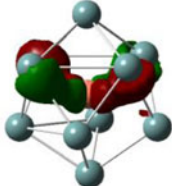
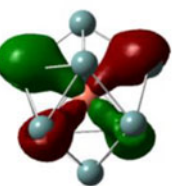
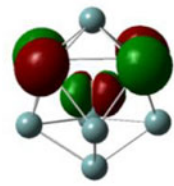
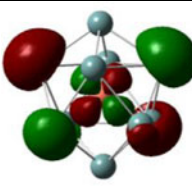
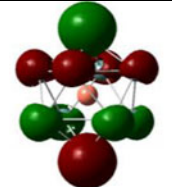
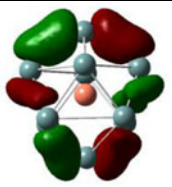
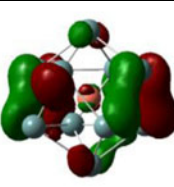
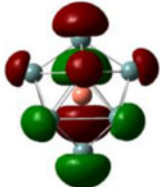
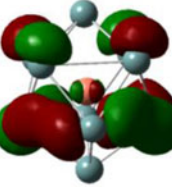
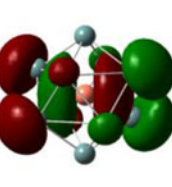
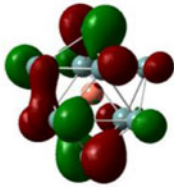
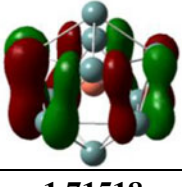
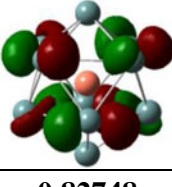
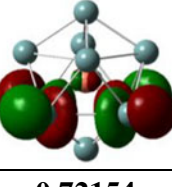
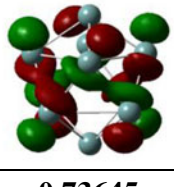
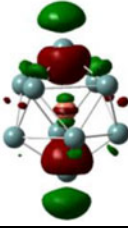
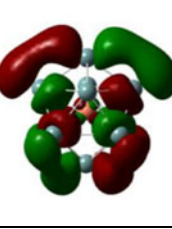
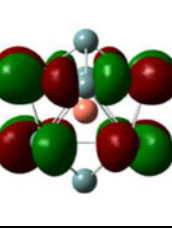
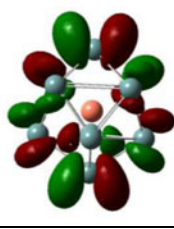
Ge	4s: s	4p: p _x	4p: p _y	4p: p _z
1				
	1.71167	0.83039	0.8327	0.6258
2				
	1.71363	0.8285	0.7384	0.71928
3				
	1.71476	0.82821	0.62894	0.82889
4				
	1.65288	0.91281	0.7251	0.72513
5				
	1.71518	0.82748	0.72154	0.73645
6				
	1.65272	0.91373	0.72526	0.72581

Fig. 1 (continued)

take the form of a rhombus with a tail, with the Cu atoms at different positions. Sometimes the tails are not in the plane of the rhombus.

Three different geometries were optimized for Ge₅Cu. Their structures are similar and their optimized energies are also very close to each other. These structures can be obtained

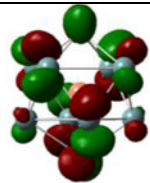
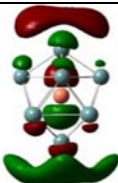
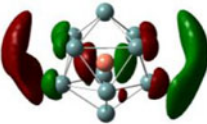
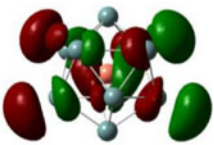
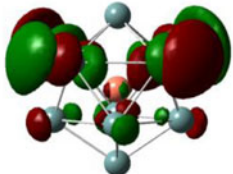
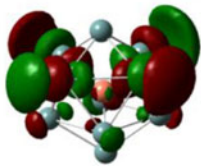
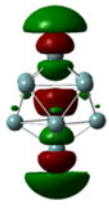
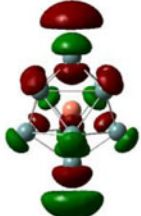
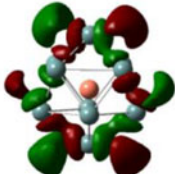
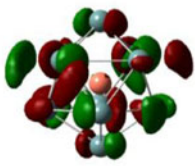
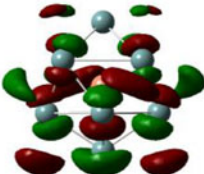
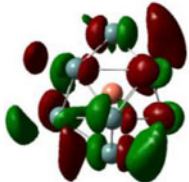
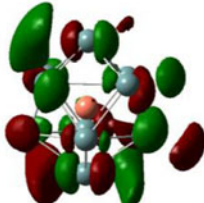
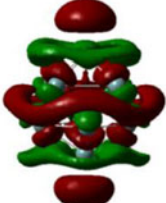
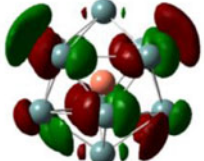
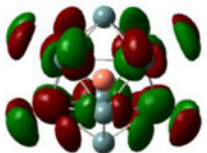
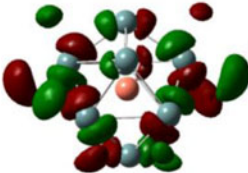
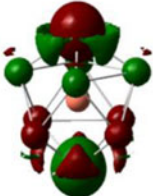
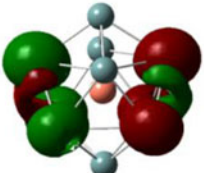
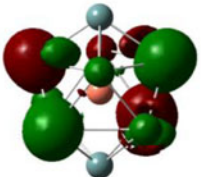
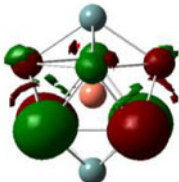
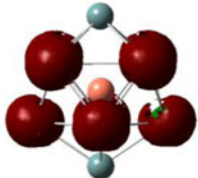
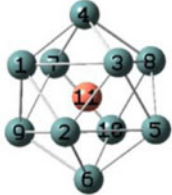
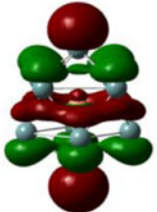
7				
	1.71112	0.83098	0.62527	0.83328
8				
	1.7138	0.82858	0.83007	0.62866
9				
	1.71084	0.83101	0.72054	0.73746
10				
	1.71222	0.83	0.73556	0.72308
Cu	4s:s	3d:d_{xy}	3d:d_{xz}	3d:d_{yz}
				
	0.48412	1.96953	1.96958	1.96733
	3d:d_{x²-y²}	3d:d_{z²}	Ge₁₀Cu	HOMO
				
1.96468	1.96653			

Fig. 1 (continued)

by replacing a Ge atom by a Cu from different positions of a symmetrical bicapped rhombus-based Ge₆ structure. The new

geometries obtained following Cu substitution give optimized structures with a planar rhombus or various kinds of bent

rhombi at the base. Among these isomers, the bent rhombus structure with C_{2v} point group symmetry (5C) shown in Fig. 1a is the ground state.

Three different geometries were optimized for the next cluster size, Ge_6Cu . The first structure, 6A in Fig. 1a, is obtained by replacing a Ge atom in a side-capped Ge_7 cluster by Cu. The Ge_7 geometry can be obtained from a bicapped pyramidal Ge_6 structure with a rhombus base by side-capping it with a Ge atom. A similar kind of optimized structure (6C) is obtained by modifying the bonding of the side-capped Ge atom in the initial guessed structure. This structure is more relaxed than the 6A isomer, and is the ground state. Both of the structures have C_s point group symmetry, and the difference between their total optimized energies is negligible. The 6B structure can be obtained by capping a Ge_6 hexagonal structure with a Cu atom. The optimized structure (6B) is boat-shaped, with the Cu atom at the top vertex position above the center, as shown in Fig. 1a.

Four different isomers were optimized for Ge_7Cu . The ground-state structure 7A can be obtained from the initial guessed geometry in a similar way to the Ge_6Cu (6B) structure, but with an additional Ge cap on the other side of the Cu. Therefore, the structure is similar to a bicapped Ge_8 structure with a hexagonal base. The optimized structure of 7C is similar to that of 7A except in the position of the Cu atom, and there is also a minor difference in their optimized energies. Compared to 7C, 7A is a more relaxed structure. The optimized 7B structure is bicapped with a pentagonal base. A Ge atom caps one face of the pentagonal plane. The other side of the plane is capped by a Ge–Cu dimer. The 7D structure is similar to the cubic Ge_8 structure, but with one Ge atom replaced by a Cu. All four isomers of Ge_7Cu have C_s point group symmetry, similar to Ge_6Cu , as shown in Fig. 1a.

Several guessed Ge_8Cu structures were optimized. Among them, three optimized isomers are presented here. The other isomers are similar in structure but vary slightly in energy. The first structure, 8A, absorbs Cu atom exohedrally. In the second structure (8B), the Ge_8 matrix is not a closed structure. The guessed structure can be obtained by joining two bent pentagonal planes with a Ge–Ge arm. These two pentagons can absorb the Cu atom inside the pocket created by the pentagonal planes. The optimized geometry contains a partially endohedrally absorbed Cu, and is the ground state. The third structure (8C) absorbs the Cu atom endohedrally, and has a total optimized energy close to that of the 8A isomer. This is the smallest cluster that can absorb a Cu atom endohedrally in this series. All three structures belong to different symmetry groups, as shown in Fig. 1a.

Five different stable isomers of Ge_9Cu were optimized. The optimized energies of 9A, 9C, and 9F are very similar, and 9F is the ground-state isomer. The structure of 9A is much relaxed than those of 9C and 9F. All of these structures have C_2 point group symmetry and can absorb the Cu atom endohedrally. A

slight modification of the 8D isomer of Ge_8Cu yields the guessed structure 9A. Optimization after adding a Ge atom to any Ge–Ge side arm of the cubic 8C structure yields structure 9A. Isomer 9B is a modified bicapped pyramidal Ge_5Cu (5A) structure with a rhombus base, where four additional Ge atoms have been added as side-capped elements. The third isomer, 9D (C_s point group symmetry), is a combination of two bicapped Ge_4 -based pyramidal structures linked by a Ge–Ge side arm, where Cu substitutes one of the corner Ge atoms. The last isomer in this series, 9E, comprises a Cu atom that is adsorbed onto the surface of the Ge_9 structure. The optimized structure can be obtained by capping the opposite planes of a Ge_5 pentagon with a Ge_3 triangle and a Ge–Cu dimer, respectively.

All of the isomers of $Ge_{10}Cu$ are of a similar type except for 10E (Fig. 1a), in which the Cu atom is adsorbed onto the surface of a Ge_{10} cluster. The initial guessed geometries of the four similar isomers were different, but the optimized isomers are all kind of icosahedral, with almost the same optimized energies. Among these structures, 10C is clearly icosahedral and is the ground state. In this structure, the Cu atom bonds with all ten Ge atoms symmetrically. It has a very low electrostatic dipole moment and carries the most charge on the Cu atom among all the clusters in the series. The isomer 10E is a combination of two parallel Ge pentagonal planes and an endohedrally added Cu atom. This structure has D_{5h} symmetry. Again, in this structure, the Cu atom bonds with ten Ge atoms, but its total optimization energy is much less than the ground-state icosahedral structure 10C.

As the size of the cluster increases, the number of isomers for a particular cluster size increases exponentially, making it a challenging job to search for the ground-state cluster. For $Ge_{11}Cu$, different possible guessed geometries were optimized, and six of the lowest-energy isomers are presented in Fig. 1a. The ground-state isomer, 11A, has C_s point group symmetry. Its structure can be attained by adding a Ge atom to the icosahedral ground-state structure 10C. The next isomer, 11B, has a Cu atom that is endohedrally absorbed by a pentagonal Ge_{10} prism structure with an additional Ge atom capping the side arm of a pentagonal plane. Structure 11C is similar to 11B except that the Ge atom caps a side plane between the two pentagons, as shown in Fig. 1a. The fourth isomer, 11D, is also an endohedrally Cu-doped $Ge_{11}Cu$ structure, where the Ge atom caps the pentagonal plane. The next isomer, 11E, is a combination of two pentagons connected by a Ge–Ge arm and six quadrilaterals to form a cage structure. Both 11D and 11E have C_s point group symmetry. The isomer 11F with C_{2v} point group symmetry is a cage structure consisting of one pentagon connected to a parallel quadrilateral and then bicapped by two Ge atoms.

Following the growth pattern of the stable isomers in the Ge_nCu series, five different stable isomers were optimized for $Ge_{12}Cu$. Among those five, three very common and important geometries are presented in Fig. 1a. The first structure shown

in the figure is a fullerene-like structure: a combination of four pentagons and four rhombi. The next is a hexagonal prism structure in which two relaxed hexagonal Ge_6 planes absorb the Cu atom endohedrally. The guessed structure of the third isomer, 12C, is a combination of two parallel pentagonal planes capped by two Ge atoms. The optimized geometry of the third isomer is icosahedral, and is the ground state for the Ge_{12}Cu composition.

For the next cluster size ($n=13$), five different isomers were optimized. The isomer 13A, shown in Fig. 1a, is a Ge-capped hexagonal Ge_{12}Cu structure. The next structure, 13B, is a combination of four pentagons and five rhombi, and is the ground-state isomer for this cluster size. All four pentagons are connected to the base rhombus. The Ge atoms positioned at the top vertex of each pentagon are connected to the topmost Ge in the 13B structure, as shown in Fig. 1a. The total optimized energy of this structure is much lower than those of the other isomers formed by capping different positions on the Ge_{12}Cu hexagonal structure with a Ge atom, and is therefore the ground-state structure. The first structure, 13A, is a relaxed structure with a capped hexagonal plane. The other three isomers were optimized by capping different side planes or side arms of the hexagonal Ge_{12}Cu structure with Ge atoms, as shown in Fig. 1a.

Three different isomeric structures were optimized for Ge_{14}Cu . The first structure, 14A, with C_s point group symmetry, is the ground-state geometry. It is a combination of six pentagons and three isolated rhombi with an additional Ge atom added to the Ge atom at the top vertex position of the 13B structure, as shown in Fig. 1a. Each rhombus is connected to four pentagons separately and a Ge–Ge dimer that links all the rhombi, and all of the pentagons are also connected to a Ge–Ge dimer. It is well known that a combination of pentagons and isolated rhombi absorbs excess strain resulting from the presence of unsaturated dangling bonds on the Ge or Si cluster surface, thus enhancing the stability of the cluster. In addition, the presence of endohedrally absorbed transition metal atom(s) also helps to improve the stability of the clusters by “tying up” the unsaturated bonds, as discussed before. The second optimized isomer, 14B, which has D_{4h} point group symmetry, adopts a symmetric bicapped hexagonal structure with a total of twelve rhombi. The other two structures, 14C and 14D, can be obtained by capping two side planes of the 13A and 13C structures with Ge atoms. Both of these structures are highly asymmetrical, and their optimized energies are also much higher than the ground-state isomer.

Adding appropriate numbers of Ge atoms to the optimized structures obtained in the range $n=12$ –14 yields eight different Ge_{15}Cu isomers (Fig. 1a). Adding one Ge atom at different vertices of the isomer 14B leads to the optimized isomers 15A and 15B. The geometry of the ground-state isomer 15A is more relaxed than that of 15B. The third structure, 15C, is a slight modification to the Ge_{10}Cu structure in which the Cu

atom is capped by two parallel pentagonal planes (10E). Adding two Ge dimers to two opposite side planes of this Ge_{10}Cu and one Ge atom between the leftover Ge–Ge side arm results in the optimized isomer 15C. Isomers 15C and 15E are similar and the difference between their optimization energies is negligible. Optimizing the initial guessed structure obtained by adding five Ge atoms to the five side arms of the pentagonal Ge_{10}Cu prism structure (10E) shown in Fig. 1a produces the stable structure 15E with the C_1 symmetry state. Another pentagonal cross-sectional tube-like isomer (15G) with an endohedrally absorbed Cu atom and C_1 point group symmetry is shown in Fig. 1a. Due to the presence of unsaturated strain at the two ends of the tube, the pentagonal end faces are not flat, whereas the middle section is almost a flat pentagonal plane with a Cu atom at the center. Optimizing after adding two Ge atoms to the two opposite Ge–Ge arms of the base rhombus in the Ge_{13}Cu structure 13B results in the optimized 15H isomer.

Eight different optimized structures are presented for the Ge_{16}Cu series. The first isomer, 16A, with C_1 point group symmetry, is an optimized structure with a modified 13A geometry capped by a Ge_3 triangle on the open hexagonal face. The next isomer, 16B, can be constructed from a hexagonal Ge_{12}Cu prism isomer where one side is capped by a Ge_3 triangular plane and the other side by a Ge atom. The total optimized energies of both of these isomers (16A and 16B) are very similar. The guessed geometry of the ground-state isomer 16C can be obtained from the isomer 14A by adding a Ge_4 rhombus in place of the top Ge–Ge dimer. This isomer has C_2 point group symmetry. Optimization after adding two Ge dimers to the two opposite side planes of the hexagonal Ge_{12}Cu prism structure yields the isomer 16F. The isomer 16G can be obtained after optimizing the tubular isomer 15G that has been capped on one side. Capping the two pentagonal planes of the isomer 13B with two Ge atoms and the base rhombus with one Ge atom leads to the isomer 16H. The isomers 16D and 16E are similar to 16H and barely differ in their optimized energies. In the isomer 16D, the central Ge atom on the hexagonal surface is positioned slightly inside the cage, but it always stays in contact with (i.e., bonded to) the Ge atoms in the hexagonal base plane, as shown in Fig. 1a.

A number of optimized isomers were optimized for Ge_{17}Cu . Among these optimized structures, eleven isomers (17A to 17K) are presented in Fig. 1a, and 17A is the ground state. 17A is obtained after adding a Ge atom to one side of the rhombus in the 16C structure. The next three cage structures 17B, 17C, and 17D can be obtained by optimizing the guessed structures that result when three Ge atoms are added to the ground-state isomer 14A at different positions. Similar to 15G, the structure of 17G is a bicapped closed tube with a pentagonal cross-section. The other six structures for this cluster size are modified 16F or 12Hexa geometries. In these modified structures, the additional Ge atom(s) cap or connect

to the 16F or 12Hexa geometries at different positions to form Ge_{17}Cu isomers.

All of the structures for Ge_{18}Cu can be explained by referencing 17E or hexagonal isomers of Ge_{12}Cu . The isomers 18A, 18B, 18C, and 18E can all be constructed from 17E by adding one Ge atom on the opposite side of the floating Ge atom and then connecting it to the other Ge atoms. Adding one more hexagonal plane to the hexagonal Ge_{12}Cu structure yields the isomer 18D, which looks like an open tube with a hexagonal cross-section. Optimization after the addition of three Ge–Ge dimers to three alternate side planes of the hexagonal Ge_{12}Cu geometry gives isomer 18F. Four different optimized isomers of composition Ge_{19}Cu are shown in Fig. 1a. The ground-state isomer 19A is obtained by adding one Ge atom to the ground-state isomer 18A. The isomers 19B and 19D are obtained by capping different hexagonal surfaces of the tubular Ge_{18}Cu structure of hexagonal cross-section with a Ge atom. The isomer 19C in Fig. 1a is the result of optimizing the guessed structure obtained by capping the hexagonal Ge_{12}Cu structure with Ge atoms at seven different positions. The ground-state isomer 20A of Ge_{20}Cu is a combination of 12 pentagons. Each side of a pentagon is connected to another pentagons, so that every pentagon is linked to five others. The next two structures, 20B and 20C, can be obtained by adding two Ge atoms to the isomer 18E in different ways. 20D can be obtained by adding eight Ge atoms to the hexagonal Ge_{12}Cu structure, or by capping the closed side of the isomer 19B with an additional Ge atom.

Upon examining the growth pattern of Ge_nCu clusters, it appears that cluster growth can be classified into three different categories. The first is Cu-capped structures where the Cu atom is added to a smaller pure-Ge cluster to form Ge_nCu . In the second category, a Ge atom in Ge_n is replaced by a Cu to form a Ge_{n-1}Cu cluster. Both of these categories are observed in the smaller cluster size range, where the cluster starts from either a Ge–Ge or a Ge–Cu dimer. A Cu or Ge atom is then directly added to Ge_n or Ge_{n-1}Cu to form a Ge_nCu cluster. In the third category, the Cu atom is partially encapsulated in the Ge_nCu cluster. Complete encapsulation of the Cu atom by the Ge cluster is seen from $n=8$ and above. After that, it is only possible to add a Ge atom to a Ge_nCu cluster to form a Ge_{n+1}Cu cluster. We discussed the formation of larger Ge_nCu clusters from smaller sizes by adding one or more Ge atom (s) earlier in this section. It was found that larger clusters prefer to retain the Cu atom as the encapsulated atom in Ge_nCu cage clusters.

Electronic structures and stabilities of Ge_nCu nanoclusters

The electronic structures and stabilities of Ge_nCu nanoclusters are discussed in this section on the basis of the variations in

some calculated physical and chemical parameters—the binding energy (BE), the HOMO–LUMO gap (or ΔE), the embedding energy (EE), the stability or the second-order difference in energy (Δ_2), the ionization potential (IP), the electron affinity (EA), and the chemical potential (μ)—with the cluster size. By monitoring the behavior of these parameters as the cluster size increases, we investigated whether or not electron counting can explain the relative stabilities of the clusters.

To explore the relative stabilities of Ge_nCu clusters with increasing n (from $n=1$ to 20), we first calculated various thermodynamic parameters of the clusters: the binding energy (BE), the embedding energy (EE), the HOMO–LUMO gap (ΔE), and the relative stability or the second-order energy difference (Δ_2).

The binding energy per atom of a cluster, following the WW rule [39], was defined as follows:

$$\text{BE} = -(E_{\text{Ge}_n\text{Cu}} - nE_{\text{Ge}} - E_{\text{Cu}})/(n + 1), \quad (1)$$

where BE is the binding energy per atom of the cluster, and E_{Ge} , E_{Cu} and $E_{\text{Ge}_n\text{Cu}}$ are the energies of Ge and Cu and the ground-state energy of the Ge_nCu cluster, respectively. The binding energies of charged clusters were also calculated using the same equation. The binding energies of different neutral and charged clusters, along with the binding energy of pure Ge clusters, are shown in Fig. 2. The graphs show a rapid increase in the average binding energy per atom of the cluster in the small size range (for $n < 7$). This is because of the thermodynamic instability of smaller clusters. For clusters of size $n > 5$, the binding energy curve increases at a relatively slow rate with n , and finally saturates for the larger clusters ($n > 10$). For neutral clusters, the binding energy per atom in the saturation region ($n=10$ –20) varies within ± 0.01 eV, with the maximum binding energy occurring at $n=10$, whereas the

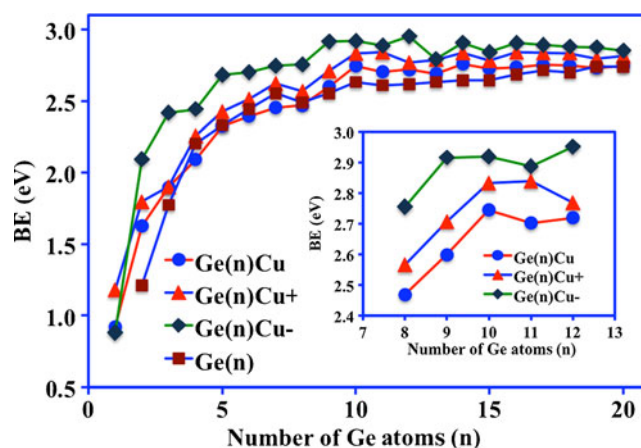


Fig. 2 Binding energies of neutral and charged Ge_n and Ge_nCu clusters as a function of cluster size

maximum binding energy is observed for anionic and cationic states at $n=9$ and $n=11$, respectively. According to the 18- or the 20-electron counting rule, the binding energy and other physical parameters (as discussed in the next section) should be highest or lowest at $n=7$ and $n=9$, respectively, for neutral clusters. Thus, electron counting does not work here, in contrast to other systems [39–41]. Therefore, to understand the detailed electronic charge distributions in the complexes, Mulliken natural bond orbital (NBO) analysis was performed, which allowed us to see how the valance electrons of Ge and Cu atoms are shared in bonds. In general, Ge is more electronegative than Cu: the electronegativities of Cu and Ge on the Pauling scale are 1.90 and 2.01, respectively. Mulliken population analysis also showed that, in this system, charge is always transferred from Cu to Ge, so Cu acts as an electron donor in Ge_nCu clusters. The results of a detailed NBO analysis of the icosahedral $Ge_{10}Cu$ structure are shown in Table 1. As mentioned before, according to the 20- or 18-electron counting rule, different physical and chemical parameters that can explain the thermodynamic and chemical stabilities of the clusters should show local or global peaks (maxima) or dips (minima) at $n=9$ or 7 for neutral Cu-doped Ge clusters. However, according to our theoretical calculations, these parameters does not show any maxima or minima at $n=9$ or $n=7$. However, they do show regular behavior at $n=10$ for neutral clusters and $n=9$ (or 11) for anionic (or cationic) clusters. According to the electron-counting rule, $Ge_{10}Cu$ is supposed to be a 21-electron cluster. From Table 1, and noting the atom numbering system for the icosahedral $Ge_{10}Cu$ structure shown in Fig. 1b, it is clear that the electronic occupancies of the Ge atoms positioned in equatorial belts (1–10, excluding 4 and 6) are all the same, and the occupancies are also the same for the Ge atoms at the polar positions (4 and 6), but these occupancies are different

from those for the Ge atoms in equatorial positions. The valance orbital distributions of Ge atoms are limited to s , p_x , p_y , and p_z , whereas those for Cu include s , d_{xy} , d_{yz} , d_{zx} , $d_{x^2-y^2}$, and d_{z^2} . Figure 1b shows the contributions of these valance orbitals of Ge and Cu atoms to the HOMO of the cluster. From Table 1, it is clear that, among the 11 valance electrons of the Cu atom, a total of 10.32 electrons are used to form ten-coordinate bonding with the ten Ge atoms in the cage. Since the positions of the Ge atoms are symmetrical about the Cu atom, and 10.32 electrons are donated during the bonding with the ten Ge atoms, we can expect that (on average) the same number of electrons (1.032) will be supplied by each Ge atom in the cage to complete the bonding with the Cu atom. Therefore, using the free electron theory, we find that approximately 20 electrons are present in the cage. The remaining valance electronic charge ($11e - 10.32e=0.68e$) on the Cu atom does not take part in the bonding, and may be present in the cage as an unsaturated lone pair. More detailed NBO analysis is needed to explain how the excess charge is accommodated in the $Ge_{10}Cu$ cage. Therefore, the $Ge_{10}Cu$ cluster can be considered an almost 20-electron cluster, which shows maximum stability, as also found by studying other parameters.

The embedding energies (EEs) of the clusters were also calculated to explain their thermodynamic stabilities. The embedding energy can be defined in different ways, meaning that it can be positive or negative depending on the definition used. In the present study, the embedding energy of a cluster was defined as

$$EE = -(E_{Ge_n} + E_{Cu} - E_{Ge_nCu}) = E_{Ge_nCu} - (E_{Ge_n} + E_{Cu}) \quad (2)$$

which is always negative. As before, E_{Ge_nCu} and E_{Ge_n} are the ground-state energies of the Ge_nCu and Ge_n clusters, respectively, while E_{Cu} is the energy of the Cu atom. Applying

Table 1 Results of the NBO analysis of the neutral $Ge_{10}Cu$ cluster

Atom	Atom number (in atom numbering scheme)	Charge (e)	Number of core electrons	Valance orbital electronic occupancies			
				4s	4p	5p	Total
Ge	1	-0.267	28	1.71	2.29	0.02	4.02
Ge	2	-0.266	28	1.71	2.29	0.02	4.02
Ge	3	-0.265	28	1.71	2.29	0.02	4.02
Ge	4	-0.250	28	1.65	2.36	0.01	4.02
Ge	5	-0.265	28	1.72	2.29	0.02	4.02
Ge	6	-0.251	28	1.65	2.36	0.01	4.02
Ge	7	-0.266	28	1.71	2.29	0.02	4.02
Ge	8	-0.265	28	1.71	2.29	0.02	4.02
Ge	9	-0.267	28	1.71	2.29	0.02	4.02
Ge	10	-0.266	28	1.71	2.29	0.02	4.02
Cu	11	2.628	18	4 s	3 d		Total
				0.48	9.84		10.32

Electronic charge
 $e=1.60217646 \times 10^{-19}$ C

the WW spin-conservation rule [39], the above equation can be modified as follows:

$$EE_{\text{WW}} = {}^M E_{\text{Ge}_n\text{Cu}} - ({}^M E_{\text{Ge}_n} + {}^0 E_{\text{Cu}}), \quad (3)$$

where M is the total spin of the cluster or the atom in units of $h/2\pi$. As an example, if the cluster Ge_nCu is in a doublet state, to calculate the embedding energy we must use the energy of the Cu atom in the doublet state with that of the pure Ge cluster in either the singlet or the triplet spin state. More precisely, in this case, we choose the lower of the resulting two embedding energies. In the present calculation, all ground states of the doped clusters are doublets. Therefore, to calculate the embedding energy according to the WW spin-conversation rule, the pure Ge clusters were taken to be in either the singlet or the triplet state. If the multiplicity of the Cu atom changes from doublet to quartet, the shape of the embedding energy graph does not change; the graph is simply shifted by an amount of energy ${}^4 E_{\text{Cu}} - {}^2 E_{\text{Cu}}$. In the present calculation, the WW rule [39] was applied when using the above method to calculate the embedding energy (in order to understand the relative stability). For charged (\pm) clusters of multiplicity M , the embedding energy of such a cluster can be written as

$$EE({}^M \text{Ge}_n\text{Cu}^m) = {}^M E_{\text{Ge}_n\text{Cu}^m} - ({}^1 E_{\text{Ge}_n^m} + {}^{M\pm 1} E_{\text{Cu}}) \text{ or } {}^M E_{\text{Ge}_n\text{Cu}^m} - ({}^0 E_{\text{Ge}_n^m} + {}^M E_{\text{Cu}}). \quad (4)$$

Embedding energies as a function of the size of the cluster for both neutral and charged states are shown in Fig. 3. There is a clear local minimum for the neutral clusters in the embedding energy graph at $n=10$. Interestingly, for the anionic clusters, the embedding energy shows a local minimum at $n=9$, whereas, for the cationic clusters, the local minimum shifts to $n=11$. This also occurs—although not so prominently—in the plot of binding energy versus cluster size. Thus, both neutral and charged Ge_{10}Cu clusters show enhanced stability.

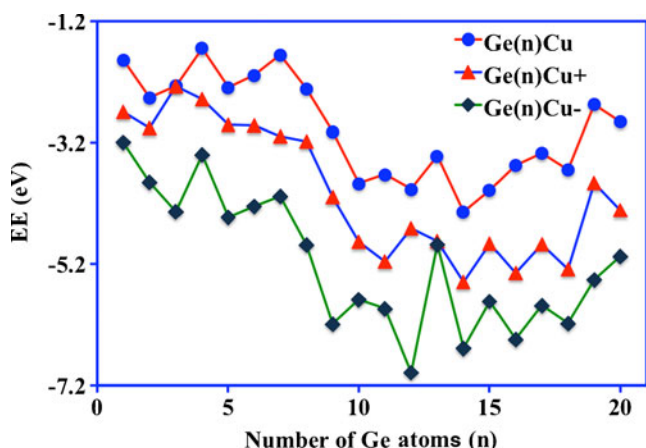


Fig. 3 Embedding energies of neutral and charged Ge_nCu clusters as a function of cluster size

To further check which is the most stable cluster in the Ge_nCu series during the growth process, Ge atoms were added to the Ge–Cu dimer one by one, and the stability parameter was calculated. The stability parameter $\Delta_2(n)$ is defined, following the work reported by Bandyopadhyay and Sen [26], as follows:

$$\begin{aligned} \Delta_2(n) &= (E_{\text{Ge}_{n+1}\text{Cu}} - E_{\text{Ge}_n\text{Cu}}) - (E_{\text{Ge}_n\text{Cu}} - E_{\text{Ge}_{n-1}\text{Cu}}) \\ &= E_{\text{Ge}_{n+1}\text{Cu}} + E_{\text{Ge}_{n-1}\text{Cu}} - 2E_{\text{Ge}_n\text{Cu}}. \end{aligned} \quad (5)$$

According to this definition, the more positive the value of $\Delta_2(n)$, the greater the stability, as it corresponds to a gain in energy during the growth process from the size immediately below, and less of a gain in energy to the next cluster size up. The stabilities of neutral and charged clusters are shown in Fig. 4. The variation in $\Delta_2(n)$ for neutral and charged clusters shows regular behavior, just as for the embedding energy. Though the stabilities of anionic clusters are positive and tend to increase with n , just like neutral and anionic clusters, they are not as stable as the cationic and neutral clusters. The peaks at $n=9, 10,$ and 11 for anionic, neutral, and cationic clusters, respectively, represent clusters with enhanced stability. In general, the clusters that are “magic” (i.e., have positive stabilities) in the neutral state remain magic in most of their charged states.

Again, to investigate the growth behavior of Ge_nCu clusters around $n=10$, the fragmentation energy (FF) or $\Delta(n, n-1)$ for each of the clusters in each growth step was calculated starting from the Ge–Cu dimer. The fragmentation energy was defined as follows:

$$\begin{aligned} \Delta(n, n-1) &= E_{\text{Ge}_n\text{Cu}} - (E_{\text{Ge}_{n-1}\text{Cu}} + E_{\text{Ge}}) \\ &= E_{\text{Ge}_n\text{Cu}} - E_{\text{Ge}_{n-1}\text{Cu}} - E_{\text{Ge}}. \end{aligned} \quad (6)$$

It is clear that there is a sharp drop in the fragmentation energy from $n=10$ to 11 in the neutral state and from $n=9$ (or 10) to 10 (or 11) in anionic (or cationic) Ge_nCu clusters,

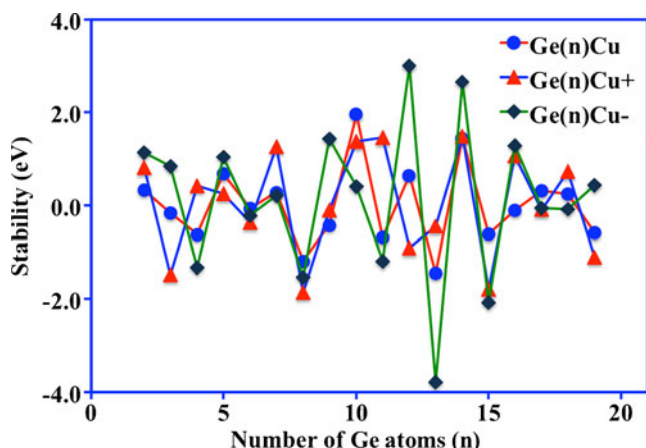


Fig. 4 Stabilities of neutral and charged Ge_nCu clusters as a function of cluster size

as shown in Fig. 5. This sharp drop in fragmentation energy for both neutral and charged clusters is an indication that the neutral cluster with $n=10$ is the most stable. Therefore, it is clear that the BE, EE, $\Delta_2(n)$, and $\Delta(n, n-1)$ all indicate that the cluster with $n=10$ has a relatively high thermodynamic stability. The charge on the Cu atom and the average charge/Ge atom as functions of the size of the cluster are shown in Fig. 6. Just as for the other parameters discussed above, the charge on the Cu or Ge atom shows a local maximum or minimum at $n=10$. This result provides further support for the calculated relative stabilities and fragmentation energies. It is clear that the charge transferred from the Cu atom to the Ge cage in the icosahedral Ge_{10}Cu structure is considerable, and this enhances the electrostatic interaction between the cage and the Cu atom, which plays an important role in stabilizing the cage structure of Ge_{10}Cu .

To study the kinetic stabilities of the clusters in a particular reactive environment, the HOMO–LUMO gap (ΔE), ionization potential (IP), electron affinity (EA), chemical potential (μ), chemical hardness (η), and polarizability (α) of each cluster were calculated. In general, as the HOMO–LUMO gap (ΔE) increased, the reactivities of the clusters decreased. The HOMO–LUMO gaps of neutral and charged clusters are plotted in Fig. 7. As also seen for other transition metal doped Si and Ge clusters [21–26], a decreasing trend was observed for the HOMO–LUMO gap with increasing cluster size for both neutral and charged clusters, with some local oscillations. There are clear local maxima at $n=10, 9$, and 11 for neutral, anionic, and cationic Ge_nCu clusters. This again indicates that the Ge_{10}Cu cluster is unusually stable.

In the present study, one of the main aims was to explain the relative stabilities of the clusters in terms of simple electron-counting rules. As reported in a previous study of metal clusters, according to the electron shell model, whenever an electron is added to a previously empty shell, the adiabatic

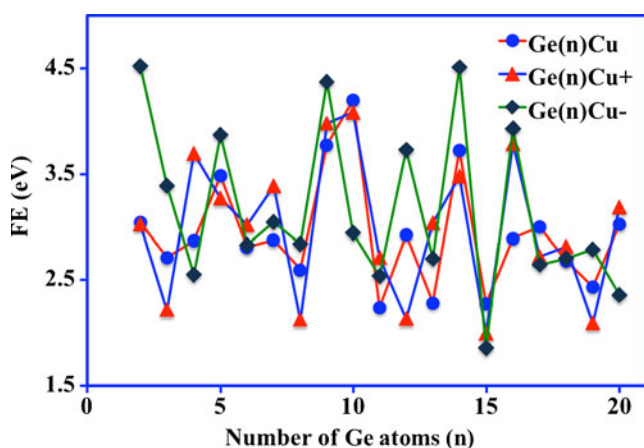


Fig. 5 Fragmentation energies of neutral and charged Ge_nCu clusters as a function of the cluster size

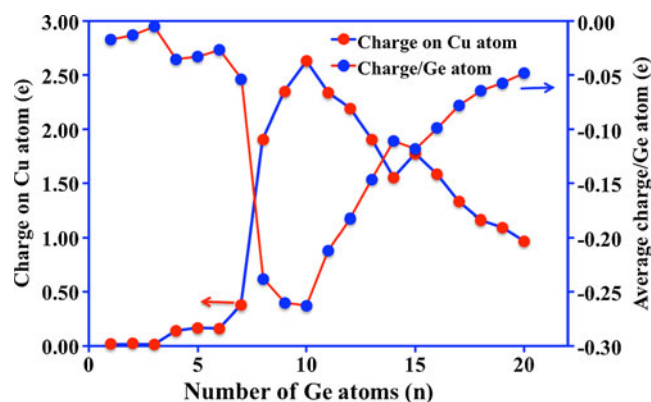


Fig. 6 Charge on the Cu atom and average charge/Ge atom in Ge_nCu as functions of the cluster size. Here, *positive and negative signs* represent the charge donated and received, respectively

ionization potential (IP) drops sharply [37]. In a report on the Li_n series, de Heer [57] showed that the L_{20} cluster is a shell field configuration, and there is a sharp drop in ionization potential when the cluster grows from L_{20} to L_{21} . If the enhanced stability of the Ge_{10}Cu cluster is due to a shell field configuration, there should be a sharp drop in ionization potential when one more Ge atom is added to this cluster. Indeed, Fig. 8 clearly shows that this is the case. There is a local peak in the ionization potential graph at $n=10$, and then a sharp drop in IP from $n=10$ to 11 . This drop in IP could be a strong indication that there is almost a free-electron gas inside the Ge_{10}Cu cage cluster. The IP of the Ge_{11}Cu cluster is in the same range as those of transition metal atoms. Hence, it may be possible to form a number of stable halides using this cluster. The discovery of such stable clusters can aid in the identification of new semiconductor–TM metal-based “superatoms” that can be used as building blocks for cluster-assembled designer materials.

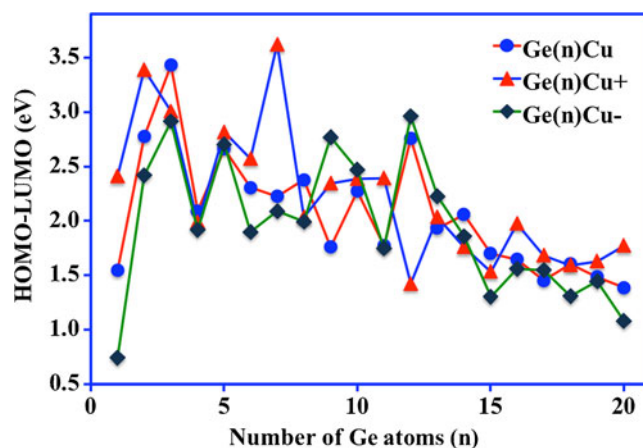


Fig. 7 HOMO–LUMO gaps of neutral and charged Ge_nCu clusters as a function of cluster size

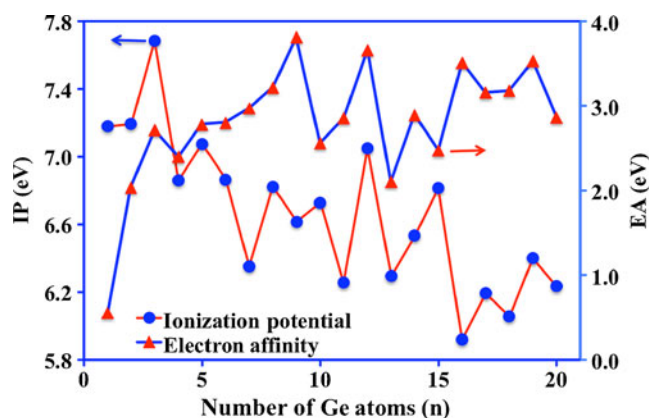


Fig. 8 Ionization potentials and electron affinities of Ge_nCu clusters as functions of cluster size

Another parameter that can help us to understand the chemical stability of a system is its electron affinity. This can be defined as

$$EA(\text{eV}) = E_{\text{Ge}_n\text{Cu}} - E_{\text{Ge}_n\text{Cu}^-}. \quad (7)$$

Based on this definition, electron affinity (EA) is always positive, and clusters with greater electron affinity are more reactive and hence less stable. The electron affinity as a function of cluster size is shown in Fig. 8, along with the ionization potentials of the clusters. In the graph, there is a local minimum at $n=10$, between two local maxima at $n=9$ and at 12. There is a hike in the electron affinity from $n=10$ to 11 that continues up to $n=12$. Then again, there is a sharp drop in the electron affinity from $n=12$ to 13. The dip in EA at $n=10$ is an indication of the enhanced stability of the Ge_{10}Cu cluster in the neutral state.

In addition to the above parameters, the maximum hardness principle (MHP) can also be used to characterize the relative stability of a system [58–60]. To verify the chemical stabilities of the clusters, the chemical potential (μ) and chemical hardness (η) of the ground-state cluster for each cluster size were calculated. The chemical potential and chemical hardness can be expressed in terms of the electron affinity and ionization potential. If $E(n_e)$ is the energy of an n_e -electron system, then the energy of the system containing $n_e + \Delta n_e$ electrons, where $\Delta n_e \ll n_e$, can be expressed as

$$E(n_e + \Delta n_e) = E(n_e) + \left. \frac{dE}{dn} \right|_{n=n_e} \Delta n_e + \left. \frac{1}{2} \frac{d^2E}{dn^2} \right|_{n=n_e} (\Delta n_e)^2 \quad (8)$$

+ higher – order terms.

Since the contribution from higher-order terms is negligible, μ and η can be defined as

$$\mu = \left. \frac{dE}{dn} \right|_{n=n_e} \quad \text{and} \quad \eta = \left. \frac{1}{2} \frac{d^2E}{dn^2} \right|_{n=n_e} = \frac{1}{2} \left. \frac{d\mu}{dn} \right|_{n=n_e}. \quad (9)$$

By definition, $\text{IP} = E(n_e - 1) - E(n_e)$ and $\text{EA} = E(n_e) - E(n_e + 1)$.

By setting $\Delta n_e = 1$, μ and η can be related to IP and EA via the following relations:

$$\mu = -\frac{\text{IP} + \text{EA}}{2} \quad \text{and} \quad \eta = \frac{\text{IP} - \text{EA}}{2}. \quad (10)$$

Consider two systems with μ_i and η_i ($i=1, 2$) that are in contact with each other, and where some electronic charge (Δq_e) is transferred from one system to the other. The quantity Δq_e and the resulting energy change (ΔE) due to the charge transfer can be determined in the following way.

If $E(n_e + \Delta q_e)$ is the energy of a system after a charge transfer, then this energy can be expressed for two different systems 1 and 2 in the following way:

$$E_1(n_{1e} + \Delta q_e) = E_1(n_{1e}) + \mu_1(\Delta q_e) + \eta_1(\Delta q_e)^2 \quad \text{and} \quad E_2(n_{2e} - \Delta q_e) = E_2(n_{2e}) - \mu_2(\Delta q_e) + \eta_2(\Delta q_e)^2. \quad (11)$$

The corresponding chemical potentials become

$$\mu'_1 = \left. \frac{dE_1(n + \Delta q_e)}{dn} \right|_{n=n_{1e}} = \mu_1 + 2\eta_1\Delta q_e \quad \text{and} \quad (12)$$

$$\mu'_2 = \left. \frac{dE_2(n - \Delta q_e)}{dn} \right|_{n=n_{2e}} = \mu_2 - 2\eta_2\Delta q_e.$$

When the systems are in chemical equilibrium, i.e., $\mu'_1 = \mu'_2$, the charge transfer and energy gain are given by the following expressions:

$$\Delta q_e = \frac{\mu_2 - \mu_1}{2(\eta_1 + \eta_2)} \quad \text{and} \quad \Delta E = \frac{(\mu_2 - \mu_1)^2}{2(\eta_1 + \eta_2)}. \quad (13)$$

In this expression, ΔE is the energy gained by the overall system (systems 1 and 2) due to the exclusive alignment of the chemical potentials of the two systems at the same value. From the expressions for Δq_e and ΔE , it is clear that charge transfer from one system to the other becomes easier as the difference in μ increases while η_1 and η_2 decrease. Therefore, ΔQ and ΔE reflect the reaction affinity between two systems. Since they are functions of the chemical potential and the chemical hardness of the system, it is important to calculate these parameters in order to gauge the chemical stability of the system in a particular environment.

Using the above theoretical background, values of the chemical potential (μ) and chemical hardness (η) of Cu-doped Ge_n clusters were calculated. If we look at Fig. 9, the chemical potential at $n=10$ shows a visible albeit not very clear peak between $n=9$ and 11. The local minimum in the chemical potential at $n=9$ is an indication that this cluster size is more stable than its neighboring cluster sizes. Figure 9 also shows that variation in chemical hardness—a measure of the chemical

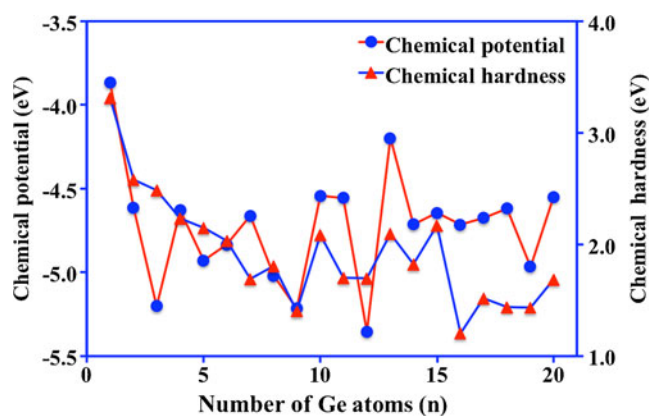


Fig. 9 Chemical potentials and chemical hardnesses of Ge_nCu clusters as functions of cluster size

reaction affinity of the cluster (for covalent bonding)—with cluster size exhibits a local maximum. This local maximum is a measure of the resistance (or “hardness”) of the electronic clouds surrounding the cluster to being shared in a chemical bond with an external species. Therefore, the peak at $n=10$ indicates that this cluster size is relatively stable. Again, to understand the effect of the chemical hardness on the polarizability, the polarizability parameter was calculated for each cluster, and the results are plotted in Fig. 10. According to the theoretical work reported by Hati and Datta [61] and Ganti and Ghosh [62], for covalent bonding, harder usually means less polarizable. Comparing the graphs of chemical hardness and polarizability in Figs. 9 and 10, the above statement appears to be true for the cluster of size $n=10$. To some extent, the electrostatic dipole moment of a cluster is also related to its atomic polarizability. However, cluster structure also plays a role here. In a symmetrical cage-like structure where the Cu atom is at the center of the cage, the electrostatic dipole moment of the cluster is usually very low, as seen for the ground-state cluster 10A for instance. The dipole moments of the clusters suddenly increase when one Ge atom is dropped or added to the cluster. The ground-state clusters within the size range $n=9$ –16

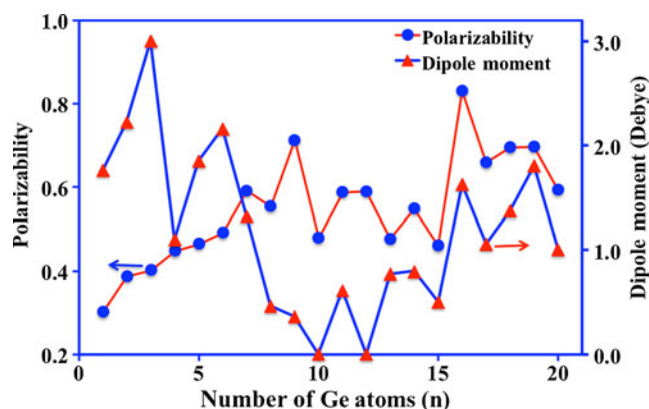


Fig. 10 Polarizabilities and electrostatic dipole moments of Ge_nCu clusters as functions of cluster size

are all cage types with an endohedrally absorbed Cu. The dipole moments of these clusters vary from 0 to 0.89 debye. The first dipole moments of the clusters studied in this work initially decrease with cluster size, show zero or very low values within the range $n=10$ –15, and then tend to increase at larger cluster sizes, when cage distortion starts to appear.

Conclusions

The theoretical study reported here investigated the growth behavior, stabilities, and the electronic and various chemical and physical properties of Ge_nCu clusters within the size range $n=1$ –20, as calculated under the spin-polarized generalized gradient approximation (GGA) proposed by Perdew and Wang (B3PW91). The calculated results can be summarized as follows:

- The growth behavior for Ge_nCu clusters shows two main patterns. In the smaller cluster size range (i.e., before the encapsulation of the Cu atom becomes possible), the Cu or Ge atom is added directly to the Ge_n or Ge_{n-1}Cu cluster to form Ge_nCu clusters, and the binding energy of the cluster increases much more rapidly than for the larger clusters. After it becomes possible for the cluster to encapsulate the Cu atom (i.e., for Ge_n clusters with $n>7$), the Ge_nCu clusters tend to grow by absorbing Ge atoms one by one on their surfaces, while retaining the Cu atom inside the cage.
- It was found that the addition of a Cu atom to a Ge cluster is always a favorable action, whatever the cluster size, as the embedding energy is negative for every neutral and charged cluster. All clusters with $n>7$ absorb Cu endohedrally into the cage of the pure Ge_n cluster.
- The relative stabilities of these clusters are rather interesting. Upon exploring the trends in the BE, EE, $\Delta(n, n-1)$, and $\Delta_2(n)$ with cluster size, it was found that neutral, anionic, and cationic clusters with $n=10$, 9, and 11, respectively, are the most stable clusters. Detailed NBO analysis, as discussed above, showed that neutral and charged clusters with nearly 20 valence electrons show enhanced stability, in agreement with shell model predictions. This is also seen in the IP values of the Ge_nCu clusters, as there is a sharp drop in IP from $n=10$ to 11. Although the stability parameter does not show variations that are as strong as those seen for the HOMO–LUMO gaps of the charged clusters, there is still a local maximum at $n=10$ in the neutral state. This is an indication that this cluster has enhanced stability, just like a 20-electron cluster. Other parameters such as the EA and the chemical potential (related to the chemical stability and hardness of the cluster) along with the polarizability and the dipole moment of the

neutral cluster with $n=10$ also support the highly stable nature of this cluster.

- As mentioned before, the drop in the adiabatic ionization potential (IP) during the growth process provides some of the strongest evidence that there is almost a free-electron gas inside the Ge₁₀Cu cage cluster. Since the IP of the Ge₁₀Cu cluster is in the same range as those of transition metal atoms, it may be possible to form a number of stable halides using this cluster. Hence, it may be possible to use this cluster to create new semiconductor–TM metal-based “superatoms” that can act as building blocks for cluster-assembled designer materials, which could open up new fields of innovation in the electronic industry. The present work is a preliminary step in this direction.

Acknowledgments Complete computations using Gaussian 03 were performed at the cluster computing facility, Harish-Chandra Research Institute, Allahabad, UP, India (<http://cluster.hri.res.in>).

References

- Brown WL, Freeman RR, Raghavachari K, Schluter M (1987) *Science* 235:860–865
- Zhang X, Li G, Gao Z (2001) *Rapid Comm Mass Spectrum* 15:1573–1576
- Khanna SN, Rao BK, Jena P (2002) *Phys Rev Lett* 89:016803–016806
- Archibong EF, St-Amant A (1998) *J Chem Phys* 109:962–972
- Benedict LX, Puzer A, Willimson AJ, Grossman JC, Galli G, Klepeis JE, Raty JY, Pankratov O (2003) *Phys Rev B* 68:85310–85318
- Ho KM, Shvartzburg AA, Pan B, Lu ZY, Wang CZ, Wacker JG, Fye JL, Jarrold MF (1998) *Nature* 392:580–582
- Shvartzburg AA, Jarrold MF (1999) *Phys Rev A* 60:1235–5
- Jarrold MF, Bower JE (1992) *J Chem Phys* 96:9180–9190
- Kumar V, Kawazoe Y (2001) *Phys Rev Lett* 87:045503–045504
- Kumar V, Kawazoe Y (2002) *Phys Rev Lett* 88:235504–4
- Bandyopadhyay D (2009) *Nanotechnology* 20:275202–275212
- Rothlisberger U, Andreoni W, Parrinello M (1994) *Phys Rev Lett* 72:665–668
- Kaxiras E, Jackson K (1993) *Phys Rev Lett* 71:727–730
- Zdetsis AD (2007) *Phys Rev B* 76:075402–075405
- Zhang D, Ma C, Lin C (2007) *J Phys Chem C* 111:17099–17103
- Kumar V, Kawazoe Y (2007) *Phys Rev B* 75:155425–11
- Beck SM (1987) *J Chem Phys* 87:4233–4234
- Beck SM (1989) *J Chem Phys* 90:6306–6312
- Hiura H, Miyazaki T, Kanayama T (2001) *Phys Rev Lett* 86:1733–1736
- Ohara M, Miyajima K, Pramann A, Nakajima A, Kaya K (2002) *J Phys Chem A* 106:3702–3705
- Bandyopadhyay D (2008) *J Appl Phys* 104:084308–7
- Bandyopadhyay D (2009) *Mol Simul* 35:381–394
- Bandyopadhyay D, Kumar M (2008) *Chem Phys* 353:170–176
- Kumar M, Bhattacharrya N, Bandyopadhyay D (2012) *J Mol Model* 18:405–418
- Bandyopadhyay D, Kaur P, Sen P (2010) *J Phys Chem A* 114:12986–12991
- Bandyopadhyay D, Sen P (2010) *J Phys Chem A* 114:1835–1842
- Gingerich KA, Schmude RW Jr, Baba MS, Meloni G (2000) *J Chem Phys* 112:7443–7448
- Negishi Y, Kawamata H, Hayakawa F, Nakajima A, Kaya K (1998) *Chem Phys Lett* 294:370–376
- Yoshida S, Fuke K (1999) *J Chem Phys* 111:3880–3890
- Wang J, Chen X, Liu JH (2008) *J Phys Chem A* 112:8868–8876
- Han JG (2000) *Chem Phys Lett* 324:143–148
- Stroppa A, Kresse G, Continenza A (2011) *Phys Rev B* 83:085201–085205
- Zhao WJ, Wang YX (2009) *J Mol Struct (THEOCHEM)* 901:18–23
- Janssens E, Lievens P (2011) *Adv Nat Sci Nanosci Nanotechnol* 2:023001–023008
- Negishi Y, Kawamata H, Hayase T, Gomei T, Kishi R, Hayakawa F, Nakajima A, Kaya K (1997) *Chem Phys Lett* 269:199–207
- Huheey JE, Keiter EA, Keiter RL (2000) In: *Inorganic chemistry: principles of structure and reactivity*, 4th edn. HarperCollins, New York
- Sen P, Mitas L (2003) *Phys Rev B* 68:155404–4
- Reveles JU, Khanna SN (2005) *Phys Rev B* 72:165413–165418
- Wigner E, Witmer EE (1928) *Z Physik* 51:859–886
- Guo LJ, Zhao G, Gu Y, Liu X, Zeng Z (2008) *Phys Rev B* 77:195417–195418
- Koyasu K, Akutsu M, Mitsui M, Nakajima A (2005) *J Am Chem Soc* 127:4998–4999
- Perdew JP, Chevary JA, Vosko SH, Jackson KA, Pederson MR, Singh DJ, Fiolhais C (1992) *Phys Rev B* 46:6671–6678
- Perdew JP, Chevary JA, Vosko SH, Jackson KA, Pederson MR, Singh DJ, Fiolhais C (1993) *Phys Rev B* 48:4978–4978
- Perdew JP, Burke K, Wang Y (1996) *Phys Rev B* 54:16533–16537
- Burke K, Perdew JP, Wang Y (1997) In: Dobson JF, Vignale G, Das MP (eds) *Electronic density functional theory: recent progress and new directions*. Plenum, New York, pp 28–111
- Dunning TH Jr, Hay PJ (1976) In: Schaefer III HF (ed) *Modern theoretical chemistry*, vol 3. Plenum, New York, pp 1–28
- Hay PJ, Wadt WR (1985) *J Chem Phys* 82:299–310
- Fuentealba P, Preuss H, Stoll H, Szentpály LV (1982) *Chem Phys Lett* 89:418–422
- Wang J, Han JG (2005) *J Chem Phys* 123:064306–064321
- Han JG, Hagelberg F (2001) *J Mol Struct (THEOCHEM)* 549:165–180
- Nagendran S, Sen SS, Roesky HW, Koley D, Grubmüller H, Pal A, Herbst-Irmer R (2008) *Organometallics* 27:5459–5463
- Lombardi JR, Davis B (2002) *Chem Rev* 102:2431–2460
- Morse MD (1993) *Chemical bonding*. In: *The late transition metals: the nickel and copper group dimers*, vol 1. JAI Inc., Greenwich
- Wang YS, Chao SD (2011) *J Phys Chem A* 115:1472–1485
- Khon W, Sham LJ (1965) *Phys Rev* 140:A1133–A1138
- Frisch MJ, Trucks GW, Schlegel HB, Scuseria GE, Robb MA, Cheeseman JR, Zakrzewski VG, Montgomery J A Jr, Stratmann RE, Burant JC, Dapprich S, Millam JM, Daniels AD, Kudin KN, Strain MC, Farkas O, Tomasi J, Barone V, Cossi M, Cammi R, Mennucci B, Pomelli C, Adamo C, Clifford S, Ochterski J, Petersson GA, Ayala PY, Cui Q, Morokuma K, Malick DK, Rabuck AD, Raghavachari K, Foresman JB, Cioslowski J, Ortiz JV, Baboul AG, Stefanov BB, Liu B, Liashenko A, Piskorz P, Komaromi I, Gomperts R, Martin RL, Fox DJ, Keith T, Al-Laham MA, Peng CY, Nanayakkara A, Challacombe M, Gill PMW, Johnson B, Chen W, Wong MW, Andres JL, Gonzalez C, Head-Gordon M, Replogle ES, Pople JA (2004) *Gaussian 03*, revision E01. Gaussian Inc., Wallingford
- de Heer WA (1993) *Rev Mod Phys* 65:611–676
- Parr RG, Chattaraj PK (1991) *J Am Chem Soc* 113:1854–1855
- Pearson RG (1987) *J Chem Edu* 64:561–567
- Ayers PW, Parr RG (2008) *J Chem Phys* 128:184108–184116
- Hati S, Datta D (1994) *J Phys Chem* 98:10451–10454
- Ghanti TK, Ghosh SK (1994) *J Phys Chem* 98:9197–9201